Desalination and Water Treatment
www.deswater.com
doi: 10.5004/dwt.2021.26727

213 (2021) 381–394
February

Removal of Ni(II) and Co(II) ions from aqueous solutions utilizing *Origanum majorana*-capped silver nanoparticles

Zahra Kazemi[a], Farzaneh Marahel[a,*], Touba Hamoule[a,b,*], Bijan Mombeni Goodajdar[a]

[a]*Department of Chemistry, Omidiyeh Branch, Islamic Azad University, Omidiyeh, Iran, emails: Farzane.marahel.fm@gmail.com (F. Marahel), Toba.Hamoula@gmail.com (T. Hamoule), Zkazemi15@yahoo.com (Z. Kazemi), bmombini@gmail.com (B.M. Goodajdar)*
[b]*Basic Science Department, Petroleum University of Technology, Ahvaz, Iran*

Received 12 March 2020; Accepted 23 October 2020

ABSTRACT

The appropriateness of synthesized *Origanum majorana*-capped silver nanoparticles in Ni(II) and Co(II) ions removal from aqueous solutions have been delineated. Numerous techniques including Brunauer–Emmett–Teller, X-ray diffraction, transmission electron microscopy, and scanning electron microscopy were used to examine the surface characteristics of the Ni(II) and Co(II) ions-loaded biomass. The maximum removal efficiency of Ni(II) and Co(II) ions was 88.6% at optimum 30 mg/L for individual ions, biosorbent dosage of 40 mg for Ni(II) and 50 mg for Co(II) ions, obtained at pH 9.0 for Ni(II), 7.0 for Co(II) ions within 60 min were considered as the ideal values for nickel and cobalt, respectively. The results showed that kinetic studies revealed that the adsorption process of nickel and cobalt followed the pseudo-second-order model (r^2 = 0.9922 for Ni(II), 0.9728 for Co(II) ions). The maximum adsorption capacities obtained from the Langmuir model were 180.0 and 130.5 mg/g for nickel and cobalt, respectively. The thermodynamic parameters including enthalpy, entropy, and Gibbs energy were calculated for the adsorption of these heavy metal ions. The thermodynamics studies revealed that the adsorption process of nickel and cobalt using *O. majorana*-capped AgNPs suitable, spontaneous, and exothermic.

Keywords: Ni(II) and Co(II) ions; Isotherms; *Origanum majorana*-capped silver nanoparticles; Sorption; Thermodynamic

1. Introduction

Larger among pollutants have been released into water, soil, and air environments over the past several decades. Among these pollutants heavy metals have long been recognized as a major pollutant of the environmental [1]. Wastewaters are contaminated from discharges of industrial and domestic in general different types of heavy metals like cobalt, nickel, cadmium, cuprum, chromium, lead, and zinc. These metals are among the most hazardous chemicals used in chemical-intensive industries. The absorption of heavy metals by living organisms is due to their excessive solubility in aquatic mediums. Ingestion of large amounts of heavy metals and their accumulation in the body if they enter the food chain can cause serious health disorders. With the help of conventional treatment techniques including ion exchange, chemical precipitation, and electrochemical removal, the process of heavy metal deletion from inorganic effluent has been carried out repeatedly. However, some drawbacks like complicated equipment, the genesis of noxious sludge, and high energy consumption have greatly made these techniques disadvantageous [2,3].

In numerous industrial activities, nickel as a hazardous heavy metal is traceable. Nickel is detectable in nickel plating, batteries, colored ceramics, kilns utilized to make alloys, or from trash incinerators and power plants.

* Corresponding authors.

Over-ingestion of nickel might develop a headache, extreme weakness, dizziness, dermatitis, lung carcinoma, respiratory distress, nasal and paranasal cancer, and osteosarcoma [3]. Nickel ions is shiny white, hard, flexible, and malleable metal. It is a far-reaching appropriation in the earth, it has a nuclear number of 28 and the maximum contaminant limit (MPCL) is 0.2 mg/L. Drinking water, by and large, contains nickel at a concentration under 10 mg/L. Accepting a day by day admission of 1.5 L of water and a level of 5–10 mg nickel/L, the mean day by day admission of the nickel from water for grown-ups would be between 7.5 to 15 mg. Nickel is utilized as a part of different structures for nickel plating, as an impetus, as a stringent and in fired coatings, and so on [4].

Cobalt poisoning as intoxication caused by excessive levels of cobalt in the human's body and its impacts are serious conditions. Cobalt and its salts are found in enamels, porcelain, acrylic paints on glass wares, grinding wheels, semiconductors, electroplating, hygrometers, and nuclear medicaments. Among the side effects of cobalt poisoning are asthma, heart, thyroid, and liver conditions. It is also irritating to the eyes and mucous membrane, causing severe discomfort in the nose, often leading to perforation of the nasal septum. The threshold limit value for cobalt fume and dust exposures is 0.1 mg/m^3 in the U.S. The use of activated carbons to remove cobalt from the water was proposed because of their high surface areas and active functional groups leading to a search for low-cost adsorbents in recent years. In the present study, MPCL prepared used as an adsorbent to remove cobalt from aqueous solutions. The adsorption of cobalt ions onto MPCL was studied in batch equilibrium conditions [5,6].

Thus, to have a safe and clean environment, the deletion of these heavy metal ions from such industrial effluents is essential. Among numerous technologies practiced for the deletion of heavy metal ions from aquatic mediums are chemical oxidation/reduction, ecological, chemical precipitation, reverse osmosis, electrodialysis, ion exchange, ultra-filtration, and adsorption [7]. Amongst the practiced technologies, the popularity of adsorption is not only due to the advantages of being simple, having a low cost, being highly efficient, and being very adaptive but also to the availability of different adsorbents [8].

Adsorption as an excellent and uncomplicated technique got better than other conventional protocols namely ion exchange, chemical coagulation, electrolysis, and biological treatments in eliminating noxious and toxic contaminations. Adsorption deserves to gain popularity because of the advantages like uncomplicated and mild operational conditions, higher efficiency, and lower waste. Also, the effectiveness of adsorption techniques in the deletion of contaminations has been confirmed. This ability and effectiveness stood out in deleting highly stable pollutions in the biological degradation process via feasible and affordable ways [9]. Thus, the extensive utilization of adsorption techniques for the deletion of numerous chemicals from aqueous solutions seems logical [10]. The physical and chemical properties of an adsorbent determine the effectiveness of an adsorption process extremely. The valuable properties are considered as follows: having high adsorption capacity, being available and recoverable, and also economical. In recent years, it was tried to eliminate specified organics from water samples by applying diverse potential adsorbents. In this connection, magnetic nanoparticles (MNPs) as unique adsorbents thanks to their small diffusion resistance, high adsorption capacity, and large surface area have extensively been noticed. Their application for instance, in the separation of chemical species like ions, dyes, environmental pollutants, gases, and metals has proven to be successful [11].

Additionally, the extensive utilization of metal nanoparticles (NPs) in recent years for the detection of heavy metal ions (detecting metal ions in environmental samples without using specialist equipment since they have size- and distance-dependent optical properties) has been reported [12]. To remove heavy metals and organic pollutants from water, many attempts have been made to produce useful adsorbents with various chemical compounds and superficial properties [13]. Metal nanoparticles have been used in a wide-ranging application in various fields. Specifically, like shapes, sizes, and compositions of metallic nanomaterials are significantly linked to their physical, chemical, and optical properties, technologies based on nanoscale materials have been exploited in a variety of fields from chemistry to medicine [14].

Synthesis of nanosilver particles gets the better of other particles in nanotechnology investigations. The inhibitory impact of silver on numerous bacterial strains and microorganisms has long been proven [15]. The popularity of silver nanoparticles among researchers is attributable to their wide range of applications. Preparation of nanoparticles, in general, is carried out by applying different expensive physiochemical methods. Since in these methods toxic chemicals are used, they are potentially hazardous to the environment and are associated with different biological risks [16]. Specifically, the application of colorimetric sensors equipped with silver nanoparticles (AgNPs) has drawn attention owing to their unique optical properties and localized surface plasmon resonance (SPR) absorption [16]. Additionally, the confirmed antimicrobial characteristics of Ag^+ ions led to the extensive application of AgNPs. Therefore, AgNPs have been utilized in the fields of pharmacy, nanomedicine, biomedical engineering, and biosensing thanks to their exclusive properties [17]. The surface functionalization and stabilization of AgNPs is crucial in sensing metal ions [18].

In this article, the characterization of *Origanum majorana*-capped AgNPs as a novel sorbent was carried out employing diverse techniques like FTIR (Fourier transform infrared spectroscopy), XRD (X-ray diffraction), and SEM (scanning electron microscopy). The application of this sorbent in this study was for the ultrasound-assisted deletion of Ni(II) and Co(II) ions from aqueous samples [19]. Consequently, preparing *O. majorana*-capped AgNPs was included in our study as a substitute for costly or noxious adsorbents for the deletion of Ni(II) and Co(II) ions from wastewater. Via studying the experimental conditions of pH of solution, contact time, initial ions concentration, adsorbent dosage, and the ions removal percentage, the optimization of all the conditions was performed. To fit the experimental equilibrium data, several isotherm models including Langmuir, Freundlich, Temkin, and

Dubinin–Radushkevich were employed. The fittingness and appositeness of the Langmuir model were shown by the results. It was shown through the study of Kinetic models (both pseudo-first-order, pseudo-second-order diffusion models) that the kinetics of the adsorption process is controlled by the pseudo-second-order model. The effectuality of *O. majorana*-capped AgNPs in deleting the heavy metals of Ni(II) and Co(II) ions from wastewater was proven.

2. Experimental

2.1. Instrumentation

The applied instruments were as follows atomic absorption spectrophotometer "Shimadzu 6800" with air-acetylene flame equipment (Shimadzu Company, Japan). Fourier transform infrared (FT-IR) spectra were registered on a PerkinElmer (FT-IR spectrum BX, Germany). Scanning electron microscopy (SEM: KYKY-EM 3200, Hitachi Firm, China) under an acceleration voltage of 26 kV) used to study the morphology of samples. Transmission electron microscopy images (TEM) were taken on a (TEM, JEOL, Hitachi Company, China). For the measurement of pH, the pH/Ion meter (model-728, Metrohm Firm, Switzerland, Swiss) was employed. Laboratory glasswares were put overnight in 10% nitric acid solution. To set the temperature, A NBE ultra thermostat (VEB Prufgerate – Werk Medingen, Germany) was utilized.

2.2. Reagents and materials

All chemicals comprising of $Ni(NO_3)_2{\cdot}6H_2O$ and $Co(NO_3)_2{\cdot}6H_2O$, silver nitrate ($AgNO_3$), sodium hydroxide, hydrochloric acid in their pure form were provided from Merck Co., (Darmstadt, Germany). Also provided Ni(II) and Co(II) ions, and methanol. The preparation of solutions was done using double distilled water.

2.3. Synthesis of O. majorana-capped Ag NPs

Silver nanomaterials have a variety of applications and in different areas from medical equipment to electronic devices or in paintings and coatings, in soaps and detergents were used with different sizes and shapes [20]. Thus, in enhancing silver nanomaterials use in mentioned applications knowing distinct physical, optical, and chemical properties of them are essential. From this perspective, in their synthesis considering the ensuing details of the materials are crucial: (1) surface property, (2) size distribution, (3) apparent morphology, (4) particle composition, and (5) dissolution rate.

Based on the method in the literature, the preparation of *Oiganum majorana*-capped Ag NPs was done by the abatement of $AgNO_3$ applying as a modifier [21]. In summary, in a reaction flask which contained 90.0 mL of $AgNO_3$ (0.1 mM) solution, 10.0 mL of *O. majorana* (0.1 mM) solution was added and stirred vigorously. After 15 min, was poured into the above solution at ambient temperature and stirred for 1 h. A photo inset of UV-visible spectrum of *O. majorana*-capped Ag NPs was provided. The formation of *O. majorana*-capped Ag NPs was proven by changing the color of the colloidal solution from dark to bright yellow. To guarantee the stability of the *O. majorana*-capped Ag NPs solution for several weeks, it was stored in absence of light and at 4.0°C ± 2.0°C, to remain stable for several weeks (Fig. 1).

2.4. Adsorption of Ni(II) and Co(II) ions onto O. majorana-capped Ag NPs

In the company of ultrasound, a batch process utilizing *O. majorana*-capped AgNPs was used for binary sorption of Ni(II) and Co(II) ions. All experiments were carried out in cylindrical glassware by adding 0.05 g of sorbent to 10 mL of Ni(II) ions and Co(II) ions considering PH 9.0 and 7.0, respectively, for them as desired values. The glassware was submerged in an ultrasonic bath for 60 min at ambient temperature and afterwards the centrifugation of the solution was done. Then with a help of atomic absorption spectrophotometer Shimadzu 6800 equipped with an air-acetylene flame for Ni(II) and Co(II) ions, the ascertainment of non-adsorbed ions (both) contents was performed.

2.5. Batch adsorption Ni(II) and Co(II) ions adsorption process

Batch adsorption tests were performed to ascertain both the Ni(II) and Co(II) ions adsorption isotherm onto *O. majorana*-capped AgNPs composite and its thermodynamic features. 100 mL solution containing 100 mg/L concentration of Ni(II) and Co(II) ions was provided and with the help of 0.01N HCl/0.01N NaOH, the adjustment of the initial pH was done without any further adjustments during the tests. In ten 100 mL flasks, 10 samples of 50 mL solution with fixed sorbent dose of 30 mg/L were set. The 10 mentioned flasks with a help of an orbital shaker were agitated at a constant rate of 180 rpm at a temperature was maintained at 25°C. At fixed time intervals (10, 20, 30, 40, 50, 60, 70, and 80 min), one by one the sample flasks were picked from orbital shaker and were analyzed for determining the remained metal ions in the aqueous solution. Via using Whatman No. 42 filter paper, the filtration of *O. majorana*-capped AgNPs from aqueous solution was performed. The concentration of Ni(II) and Co(II) ions in solution samples was ascertained utilizing a "Shimadzu 6800 atomic absorption spectrophotometer" equipped with an air-acetylene flame. The ensuing equation was employed for estimating metal deletion (%A) or deletion efficiency of metal ions:

$$\%A = \frac{C_0 - C_e}{C_t} \times 100 \tag{1}$$

where C_0 in the aforementioned formula refers to the initial concentration of Ni(II) and Co(II) ions in solution (mg/L), and C_e represents the final concentration of Ni(II) and Co(II) ions in the aqueous solution (mg/L). The following equation was employed for determining the amount (mg/g) of Ni(II) and Co(II) ions adsorbed at equilibrium:

$$q_e = \frac{\left(C_0 - C_e\right)V}{W} \tag{2}$$

where C_0 (mg/L) in the formula refers to the initial ions concentration and C_e (mg/L) represents the equilibrium ions

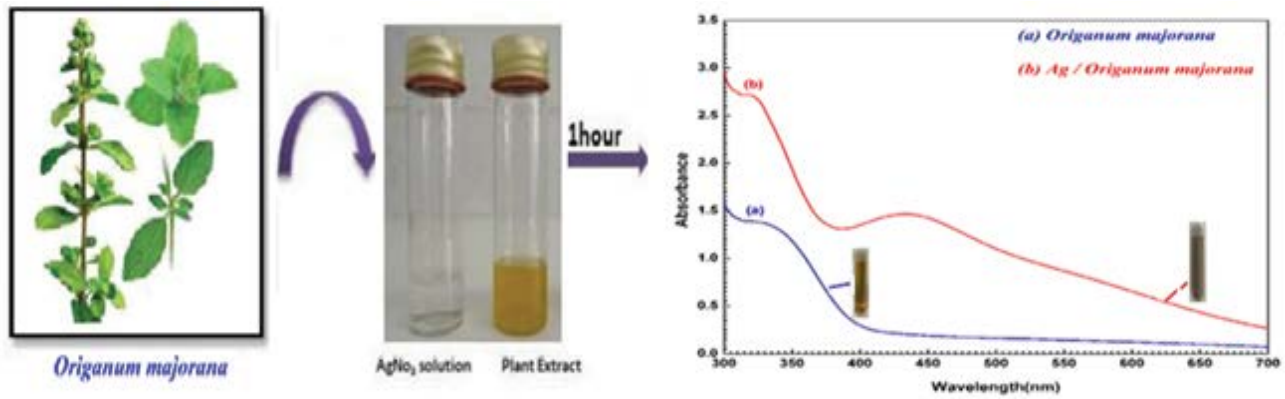

Fig. 1. Synthesis of *Origanum majorana*-capped AgNPs.

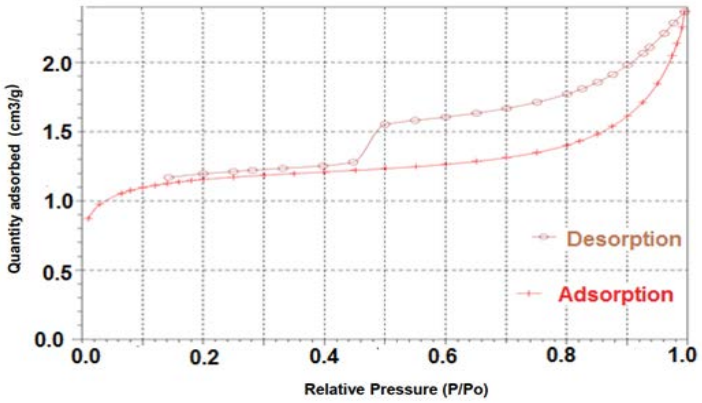

Fig. 2. N_2 adsorption–desorption isotherms of *Origanum majorana*-capped AgNPs.

concentration in an aqueous solution. *V* (L) shows the solution volume and *W* (g) signifies the adsorbent mass.

3. Results and discussion

3.1. Characterization of adsorbent

Bulk density, surface area, and loss of mass on ignition are shown in Table 1 and Fig. 2. The bulk density affects the rate of adsorption of Ni(II) and Co(II) ions solution *O. majorana*-capped silver nanoparticles. In the present study, the bulk density was less than 2.0 indicating that the activated carbon materials are in fine nature and hence enhanced the adsorption of Ni(II) and Co(II) ions solution from aqueous solution. The moisture content (0.5%) was determined, even though it does not affect the adsorption power, dilutes the adsorbents, and therefore necessitates the use of the additional weight of adsorbents to provide the required weight [22].

Fig. 3 clearly shows the FTIR spectrum of *O. majorana*-capped AgNPs nanoparticles loaded on activated carbon. The wide signals at ≤900 and 1,048 in Ag–O, 1,386–1,422 cm^{-1} are ascribable to C–H stretching from *O. majorana*-capped AgNPs, and the ones at 1,634 cm^{-1} to C=O bonds. The appeared signal at 2,027 cm^{-1} is relative to C–H stretching while the one at 3,412 cm^{-1} is attributed to –OH stretching [23]. Fig. 4, energy-dispersive spectroscopy (EDX) spectrum of (a). The EDX transmittance spectrum of the prepared *O. majorana* and (b) EDX spectrum recorded from a film, after the formation of silver nanoparticles. Different X-ray emission peaks are *Oiganum majorana*-capped silver nanoparticles. the adsorption of Ni(II) and Co(II) ions and based on Fig. 5a which is the XRD pattern of the *O. majorana*-capped AgNPs, the signals at 38.07 (111), 44.26 (200), 64.43 (220), and 77.35 (311) are ascribable to diffractions and reflections from the carbon atoms [24]. The perfect crystalline nature of the material was proven after functionalizing with *O. majorana*-capped AgNPs however the great intensity of the signal at 38.07 (111) confirmed that there has been a slight amount of material in an amorphous state. The

Table 1
Characteristics of the *Origanum majorana*-capped silver nanoparticles

Parameter	Value
pH	7.0
Moisture (%)	0.5
Bulk density (gm/L)	0.46
Surface area (m^2/g)	250
Particle size range (μm)	52–250
Loss of mass on ignition	0.6923

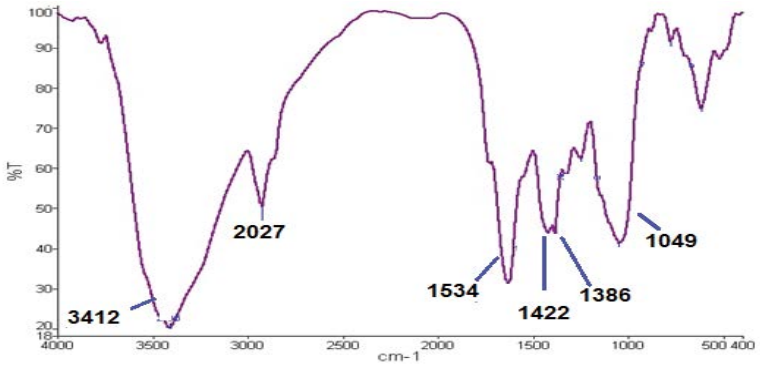

Fig. 3. FT-IR transmittance spectrum of the prepared *Origanum majorana*-capped AgNPs.

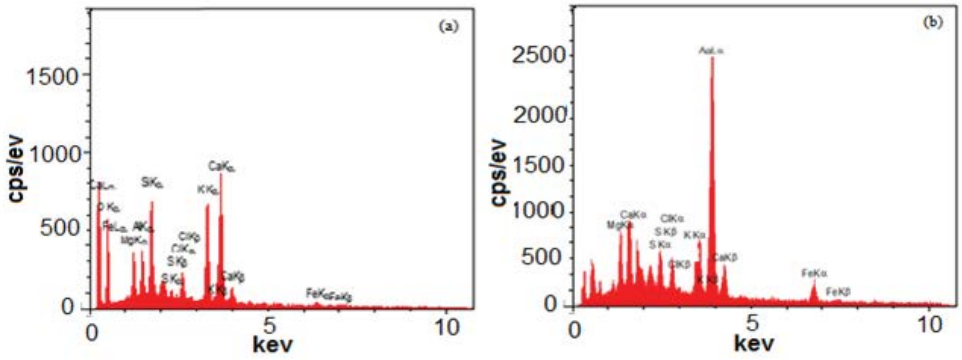

Fig. 4. (a) EDX transmittance spectrum of the prepared *Origanum majorana* and (b) EDX spectrum recorded from a film, after formation of silver nanoparticles. Different X-ray emission peaks are *Origanum majorana*-capped silver nanoparticles.

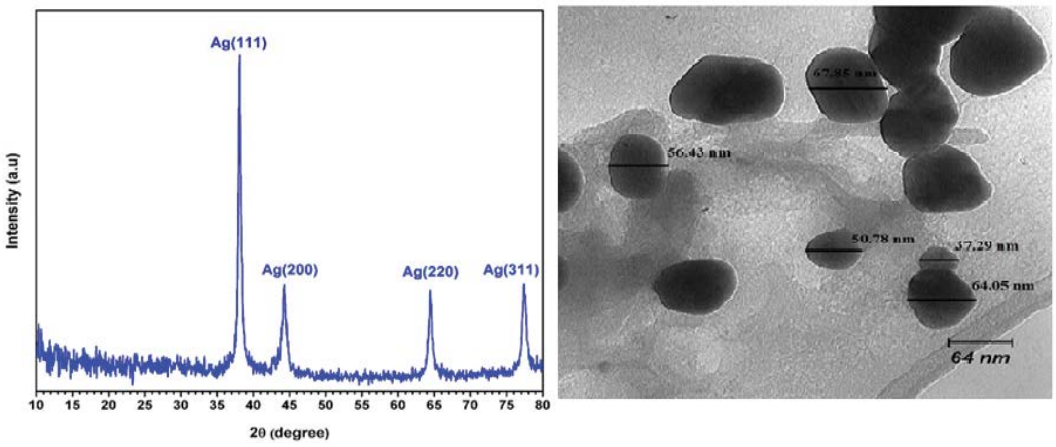

Fig. 5. (a) XRD image and (b) TEM of the prepared *Origanum majorana*-capped AgNPs.

perfect synthesis of *O. majorana*-capped AgNPs is obvious through looking at the XRD pattern. In Fig. 6, the morphological properties of the samples scrutinized by SEM are exhibited. By looking at Fig. 6, the smoothness, homogeneity, and tidiness of *O. majorana*-capped AgNPs are confirmed. Even uniformity size distribution is observable in Fig. 6. After surface modification, the *O. majorana*-capped AgNPs became uneven, larger, and bundled [25].

3.2. Impact of pH on metal ion biosorption

The effectiveness of pH as a critical factor in ions sorption has been identified. As shown in Fig. 7, the impact of pH on adsorption of Ni(II) and Co(II) ions onto *O. majorana*-capped AgNPs has been examined at pH range of 3.0–10.0. It became apparent that pH 9.0 led to the maximum biosorption of Ni(II) ions and pH 7.0 led to the maximum biosorption of Co(II). Therefore, these pH values were

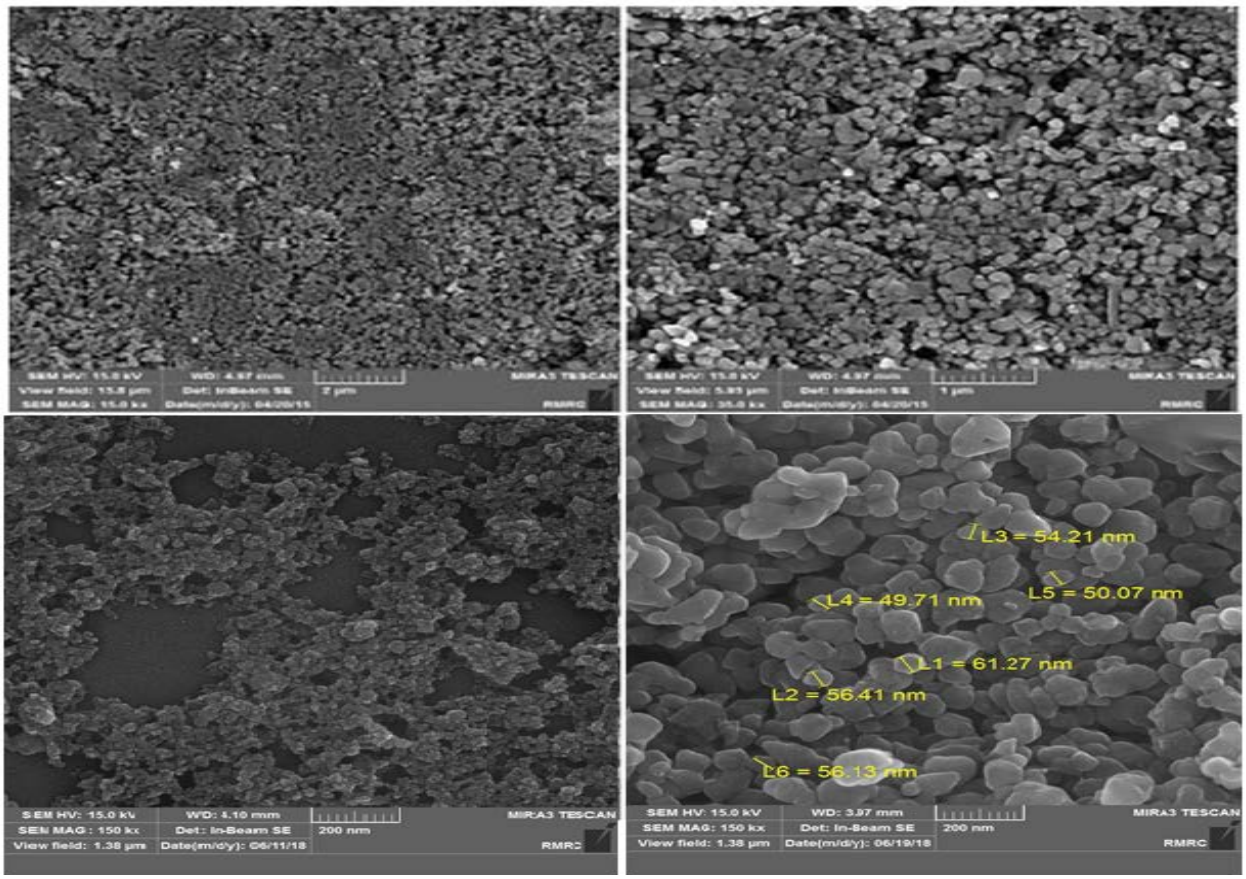

Fig. 6. SEM image of the prepared *Origanum majorana*-capped AgNPs.

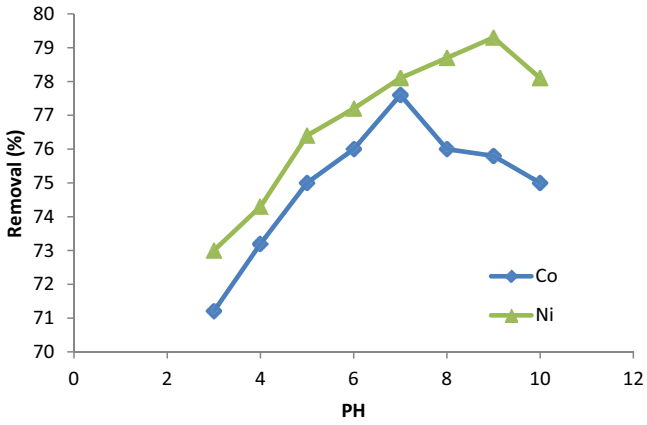

Fig. 7. Impact of initial solution pH on the sorption quantity of Ni(II) and Co(II) ions onto *Origanum majorana*-capped AgNPs. [Ni(II) and Co(II) ions concentration = 30 mg/L, adsorbent dose = 0.05 g, contact time = 60 min, stirring speed = 180 rpm, and temperature = 25°C].

picked for doing the remaining all biosorption experiments. The physio-chemical nature of the interaction was reflected by the biosorption mechanisms on the *O. majorana*-capped AgNPs surface [26,27]. When the whole surface charge on the active sites became positive at highly acidic pH, both ions (Ni(II) and Co(II)) and protons strived for binding sites on *O. majorana*-capped AgNPs which led to lower uptake of Ni(II) and Co(II) ions. As the pH solution rose from pH 9.0 and pH 7.0, the biosorbent surface was more negatively charged for Ni(II) for Co(II) ions. At the exact pH values (pH 9.0 for Ni(II) and pH 7.0 for Co(II)), deprotonation of the functional groups of the *O. majorana*-capped AgNPs provided the sites for sorption of Ni(II) and Co(II) ions. At higher pH = 9 and 7, abatement in biosorption yield for the Ni(II) and Co(II) ions was first relative to the formation of soluble hydroxylated complexes of the Ni(II) and second to the ionized nature of the *O. majorana*-capped AgNPs of the biosorbent. Prior investigations also confirmed that the maximum biosorption efficiency of Ni(II) and Co(II) ions on biomass was observed at pH (9.0 and 7.0).

3.3. Impact of biosorbent dose

Since the capacity of a biosorbent for a given initial ions concentration is determined by the biosorbent dosage, it is considered as a crucial parameter. Therefore, biosorption efficiency for Ni(II) and Co(II) ions as a function of biosorbent dosage was inquired into. Based on what is shown in Fig. 8, the percentage of the metal sharply rose with the biosorbent loading up to 40 and 50 mg. This phenomenon is explicable by the fact that while the number of available sites for biosorption raised by boosting the sorbent dose, the biosorption sites remained unsaturated

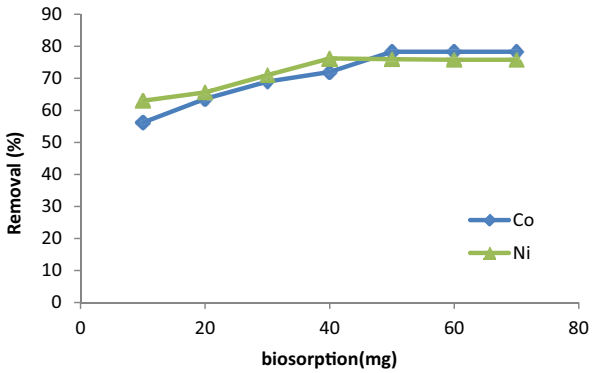

Fig. 8. Impact of dosage *Origanum majorana*-capped AgNPs on the adsorption quantity of Ni(II) and Co(II) ions. [Ni(II) and Co(II) ions concentration = 30 mg/L, pH = 9.0 Ni(II) ion and pH = 7.0 Co(II) ion, contact time = 60 min, stirring speed = 180 rpm, and temperature = 25°C].

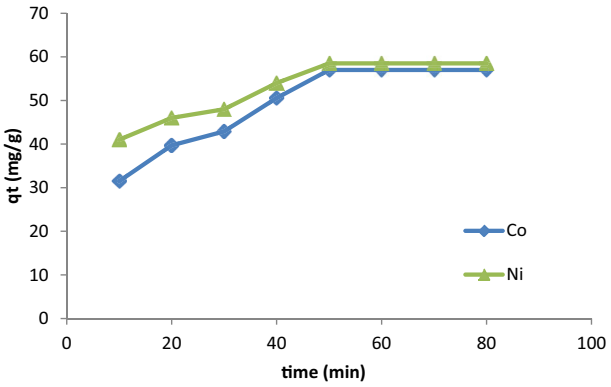

Fig. 9. Impact of contact time on the sorption of Ni(II) and Co(II) ions by *Origanum majorana*-capped AgNPs. [Ni(II) and Co(II) ions concentration = 30 mg/L, pH = 9.0 Ni(II) ion and pH = 7.0 Co(II) ion, adsorbent dose = 0.05 g, stirring speed = 180 rpm, and temperature = 25°C].

during the reaction [28]. At biosorbent dosages of 40 and 50 mg, the perfect biosorption was achieved. Therefore, 50 mg was picked as the perfect biosorbent dosage for further experiments. This is explainable in this way that when the biosorbent ratio is small, the active sites on the surface of *O. majorana*-capped AgNPs for binding with metal ions is less, thus the biosorption efficiency is low. Upon the increase in biosorbent dose, more active sites are available to bind with Ni(II) and Co(II) ions, so it leads to a boost in the biosorption efficiency until saturation.

3.4. Impact of contact time

In Fig. 9, the impact of contact time on the sorption capacity of Ni(II) and Co(II) ions onto *O. majorana*-capped AgNPs is demonstrated. Upon the boost in the initial Ni(II) and Co(II) ions concentration from 30 mg/L, the quantity of Ni(II) and Co(II) ions adsorbed onto *O. majorana*-capped AgNPs increased. The experiment was done at 80 min contact time, pH value 9 for Ni(II) ions and pH value 7 for Co(II) ions, 40 mg Ni(II) and 50 mg Co(II) ions adsorbent dosage and the constant temperature of 298.15 K. The rise in loading capacity of *O. majorana*-capped AgNPs with enhancing initial ions concentration could be due to higher interaction between Ni(II) and Co(II) ions and the sorbent [29]. Based on the obtained results, during the first 60 minutes a boost in adsorbed amount of Ni(II) and Co(II) ions was observed. In prior investigations, similar results were recorded for deletion of hazardous contaminants from wastewater.

3.5. Impact of temperature

To investigate the impacts of temperature on the sorption of Ni(II) and Co(II) ions by *O. majorana*-capped AgNPs, the temperatures from 298.15 to 328.15 K were selected for performing the experiments. The impact of temperature on the sorption of ions on *O. majorana*-capped AgNPs is demonstrated in Fig. 10. It became apparent that the equilibrium sorption capacity of Ni(II) and Co(II) ions onto *O. majorana*-capped AgNPs increased with temperature

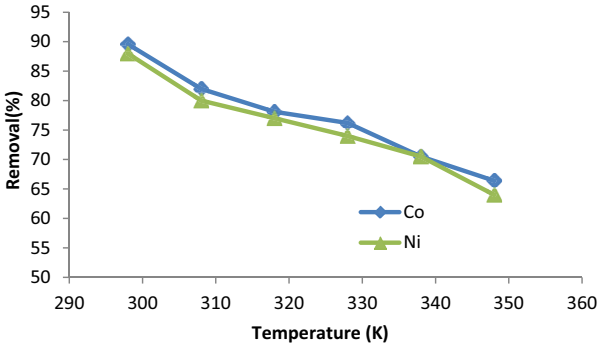

Fig. 10. Impact of temperature on the sorption quantity of Ni(II) and Co(II) ions onto *Origanum majorana*-capped AgNPs. [Ni(II) and Co(II) ions concentration = 30 mg/L, pH = 9.0 Ni(II) ion and pH = 7.0 Co(II) ion, adsorbent dose = 0.05 g, contact time = 60 min, and stirring speed = 180 rpm].

boosting. This fact confirmed that temperature boosting could boost the mobility of Ni(II) and Co(II) ions. Furthermore, the viscosity of ions solution decreased with temperature boosting and as a result, it enhanced the rate of diffusion of ions molecules. Since adsorbent is porous in nature and possibilities of diffusion of adsorbate cannot be ruled out, therefore, increase in the sorption with the rise of temperature may be diffusion controlled which is an endothermic process, the rise of temperatures favors the adsorbate transport within the pores of adsorbent. The outcomes confirmed with the impact of the solution pH, and temperature on adsorption behavior of reactive Ni(II) and Co(II) ions onto *O. majorana*-capped AgNPs [30].

3.6. Biosorption isotherms

An adsorption isotherm expresses the fraction of adsorbate molecules which are divided up between liquid and solid phases at equilibrium. With a help of four adsorption isotherms: (1) Langmuir, (2) Freundlich, (3) Temkin, and (4) Dubinin–Radushkevich isotherms, adsorption of Ni(II) and Co(II) ions onto *O. majorana*-capped AgNPs was displayed.

3.7. Adsorption equilibrium study

The design of the adsorption equilibrium isotherm was done using mathematical relation of the quantity of adsorbed target per gram of sorbent (q_e (mg/g)) to the equilibrium non-adsorbed quantity of ions in solution (C_e (mg/L)) at distinct temperature [12,31]. Approved models of Langmuir, Freundlich, Temkin, and Dubinin–Radushkevich based on desired conditions were used for isotherm studies. Langmuir model as the most frequent one by ensuing equation was used:

$$q_e = \frac{Q_m K_L C_e}{1 + K_L C_e} \tag{3}$$

where C_e, represents the concentration of adsorbate at equilibrium (mg/L), Q_m refers to the highest monolayer sorption capacity (mg/g), and K_L shows Langmuir constant (L/mg). C_e/q_e was plotted against C_e. The calculation of parameters of Q_m, K_L, and R^2 was performed based on the slope and intercept of such lines and exhibited in Table 2, From the intercept and slope of the plot of C_e/q_e vs. C_e, the values of Q_m (theoretical max sorption capacity (mg/g)) and K_a (the Langmuir adsorption constant (L/mg)) were acquired. For the interpretation of the experimental data over the whole concentration range, the Langmuir model was proven to be the best since it provided a high correlation coefficient at all adsorbent masses. The rise in the quantity of sorbent led to a remarkable boost in the quantity of adsorbed ions. The calculation of K_F and the capacity of the adsorption (parameters of the Freundlich isotherm model) were done from the intercept and slope of the linear plot of $\ln q_e$ vs. $\ln C_e$. The Temkin isotherm model was used for the evaluation of the heat of the adsorption and the adsorbent–adsorbate interaction. In the aforementioned model, B refers to the Temkin constant, t shows the heat of the adsorption (J/mol), T stands for the absolute temperature (K), R represents the universal gas constant (8.314 J/mol K) and K is the equilibrium binding constant (L/mg). For estimating the porosity, apparent free energy, and the properties of adsorption, the D–R model was employed [32,33]. In this model B (mol²/kJ²) is a constant that shows the adsorption energy, Q_s (mg/g) represents the theoretical saturation capacity, and E stands for the Polanyi potential. B is obtained from the slope of the plot of $\ln q_e$ vs. ε^2 and the Q_s value is obtained from its intercept. The fact that the ions deletion isotherm could perfectly be expressed by the Langmuir model in (Fig. 11 and Table 3) was proven from the linear adjustment between the plot of C_e/q_e vs. C_e and computed correlation coefficient (R^2) for the Langmuir isotherm model. Therefore, the fact that the adsorption of ions occurs at specified homogeneous sites as a monolayer on to the *O. majorana*-capped AgNPs surface was confirmed.

3.8. Kinetic study

Different parameters like the state of the solid (mostly with the nonuniform reactive surface) and physicochemical

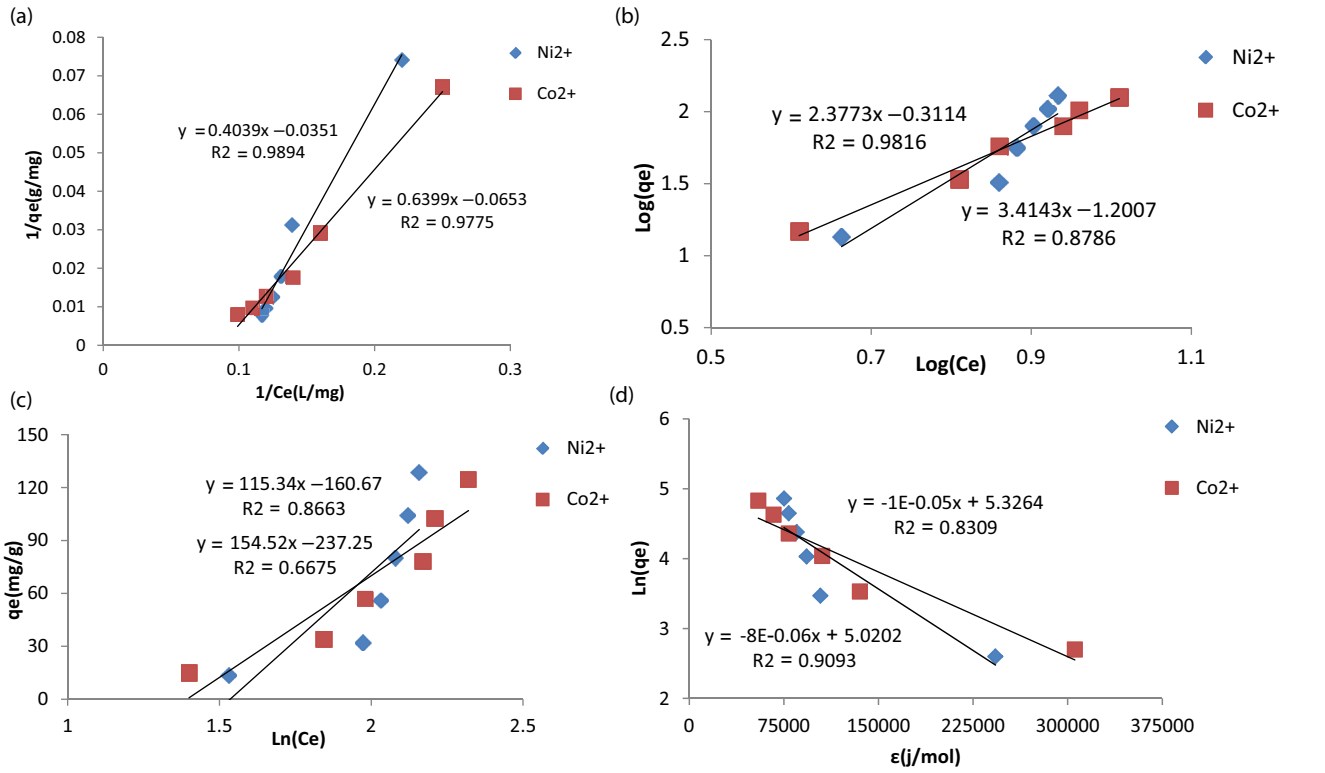

Fig. 11. Impact of (a) Langmuir, (b) Frendlich, (c) Temkin, and (d) Dubinin–Radushkevich isotherms on the sorption quantity of Ni(II) and Co(II) ions on *Origanum majorana*-capped AgNPs. [pH = 9.0 Ni(II) ion and pH = 7.0 Co(II) ion adsorbent dose = 0.05 g, contact time = 60 min, stirring speed = 180 rpm, and temperature = 25°C].

Table 2
Characterization of *Origanum majorana* and *Origanum majorana*-capped AgNPs

Characterization		Samples	
		Origanum majorana	*Origanum majorana*-capped AgNPs
BJH adsorption summary	Surface area (m^2/g)	88.254	107.254
	Correlation coefficient	0.9992	0.9963
	Surface area (m^2/g)	88.5095	88.2718
	Pore volume (m^3/g)	0.5076	0.5036
	Pore diameter (Å)	98.316	98.087
BJH adsorption summary	Surface area (m^2/g)	80.679	80.283
	Pore volume (m^3/g)	0.5598	0.5519
	Pore diameter (Å)	51.830	51.470

Table 3
Diverse isotherm constants and correlation coefficients computed for the sorption of Ni(II) and Co(II) ions onto *Origanum majorana*-capped AgNPs. [pH = 9.0 Ni(II) ion and pH = 7.0 Co(II) ion, adsorbent dose = 0.05 g, contact time = 60 min, stirring speed = 180 rpm, and temperature = 25°C]

Isotherm	Equation	Parameters	Value of parameters For Ni^{2+}	Value of parameters For Co^{2+}
Langmuir	$q_e = q_m bC_e/(1 + bC_e)$	Q_m (mg/g)	180.0	130.5
		K_L (L/mg)	0.09	0.018
		R^2	0.9884	0.9775
Freundlich	$\ln q_e = \ln K_F + (1/n)\ln C_e$	n	0.42	0.8
		K_F $(mg)^{1-n}$ L^n/g	2.05	1.7
		R^2	0.9816	0.8786
Temkin	$q_e = B_T \ln K_T + B_T \ln C_e$	B_T	115.34	215.92
		A_T (L/mg)	4.03	4.723
		R^2	0.8663	0.6675
Dubinin–Radushkevich (DR)	$\ln q_e = \ln Q_d - B\varepsilon^2$	Q_d (mg/g)	151.44	60.5
		$K_D \times 10^{-6}$ $(mol/J)^2$	8.0	7.0
		E (kJ/mol)	–247.5	–264.58
		R^2	0.9093	0.8309

conditions under which the adsorption took place can strongly influence the adsorption of a solute by a solid in an aqueous solution via complicate stages [34]. The rate of ions adsorption onto adsorbent was conformed to conventional models including pseudo-first (Fig. 12), pseudo-second-order (Fig. 13), and Elovich models (Fig. 14). The adsorption kinetic data were perfectly described by the Lagergren pseudo-first-order model [35]. The ensuing equation represents the Lagergren:

$$\frac{dq_t}{dt} = k_1\left(q_e - q_t\right) \tag{4}$$

where q_e stands for the adsorption capacities at equilibrium, and q_t (mg/g) refers to the adsorption capacities at time t. The rate constant of the pseudo-first-order adsorption (L/min) is represented with k_1. The plot of the $\log(q_e - q_t)$ vs. t was provided and k_1 and q_e values were ascertained utilizing the slope and intercept of the line, respectively.

$$\log\left(q_e - q_t\right) = \log q_t - \left(\frac{k_1}{2.303}\right)t \tag{5}$$

The improbability of this issue that the action could follow the first-order was proven from the fact that the intercept was not equal to q_e. When pore diffusion restricted the adsorption process, the linearity relationship between initial solute concentration and rate of adsorption was detected. Thus, the necessity to fit experimental data to another model (Table 4) became apparent. Consequently, pseudo-second-order model [36] was introduced based on the ensuing equation:

$$\frac{dq_t}{dt} = k_2\left(q_e - q_t\right)^2 \tag{6}$$

Over the interval 0 to t for t and 0 to q_t for q_t, Eq. (18) was integrated to provide:

Table 4
Kinetic parameters for the sorption of Ni(II) and Co(II) ions onto *Origanum majorana*-capped AgNPs. [Ni(II) and Co(II) ions concentration = 30 mg/L, pH = 9.0 Ni(II) ion and pH = 7.0 Co(II) ion, adsorbent dose = 0.05 g, stirring speed = 180 rpm, and temperature = 25°C]

Model	Parameters	Value of parameters for Ni(II) ions	Value of parameters for Co(II) ions
Pseudo-first-order kinetic	k_1 (min^{-1})	0.1	0.06
	q_e (calc) (mg/g)	28.2	21.4
	R^2	0.9460	0.9048
Pseudo-second-order kinetic	k_2 (min-1)	6.724	3.5
	q_e (calc) (mg/g)	61.0	54.0
	R^2	0.9922	0.9728
Elovich	β (g/mg)	0.196	0.17
	α (mg/g min)	9,817.42	367.44
	R^2	0.9721	0.9675
q_e (exp) (mg/g)		164.0	120.4

$$\frac{t}{q_t}=\frac{1}{k_2 q_e^2}+\frac{t}{q_e} \tag{7}$$

Based on what has been said, perfect outcomes for the entire sorption period were not provided by the plot of $\log(q_e - q_t)$ vs. t, while the plot of t/q_t vs. t demonstrated a straight line. The calculation of the values of k_2 and equilibrium adsorption capacity (q_e) was conducted from the intercept and slope of the plot of t/q_t vs. t (Table 4). The similarity of the estimated q_e values at different conditions like different initial ions concentrations and/or adsorbent masses to the experimental data was observed. Also, the appropriateness of this model for the explanation of experimental data was confirmed from higher R^2 values. Accordingly, the pseudo-second-order kinetic model was chosen for the adsorption of Ni(II) and Co(II) ions for the whole sorption period. The following is the intraparticle diffusion equation [37]:

$$q_t = k_{\text{dif}} t^{1/2} + C \tag{8}$$

This formula k_{dif} refers to the intraparticle diffusion rate constant (mg/(g min$^{1/2}$)) and the boundary layer thickness is shown by C. The linear form of the Elovich model is indicated as [38]:

$$q_t = \frac{1}{\beta}\ln(\alpha\beta)+\frac{1}{\beta}\ln t \tag{9}$$

In (Table 2 and Fig. 14), the intraparticle diffusion and Elovich model as well as the kinetic data from pseudo-first and pseudo-second-order adsorption kinetic models are demonstrated. A favorable concurrence between the experimental and estimated q_e values for diverse initial ions concentrations was shown by the linear plots of t/q_t vs. t. Moreover, greater correlation coefficients of the pseudo-second-order kinetic model (R^2 = 0.9922, 0.9728) for Ni(II) and Co(II) ions respectively in comparison with those of the pseudo-first-order model (R^2 = 0.9460, 0.9048) for them proved that the sorption fitted to the pseudo-second-order better than the pseudo-first-order kinetic model.

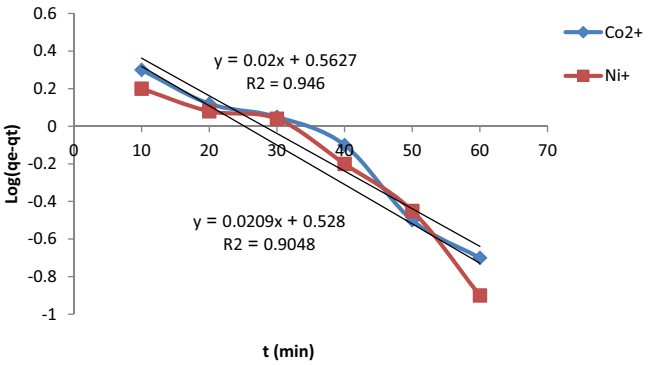

Fig. 12. Pseudo-first-order model for the sorption of Ni(II) and Co(II) ions onto *Origanum majorana*-capped AgNPs. [Ni(II) and Co(II) ions concentration = 30 mg/L, pH = 9.0 Ni(II) ion and pH = 7.0 Co(II) ion, adsorbent dose = 0.05 g, stirring speed = 180 rpm, and temperature = 25°C].

3.9. Adsorption thermodynamics

The ensuing equations were used to ascertain the thermodynamic parameters including Gibbs free energy change ($\Delta G°$), enthalpy change ($\Delta H°$), and entropy change $\Delta S°$ for the adsorption processes [39]:

$$\Delta G° = -RT\ln K_{\text{ad}} \tag{10}$$

$$\ln K_{\text{ad}} = \frac{\Delta H°}{RT}+\frac{\Delta S°}{R} \tag{11}$$

From a plot of $\ln K_e$ against $1/T$ a graph (Fig. 15) was provided. Then $\Delta G°$ was obtained from the slope of that graph. Tables 4 and 5 contain a synopsis of the thermodynamic parameter results for the adsorption of Ni(II) and Co(II) ions onto derived *O. majorana*-capped AgNPs at diverse temperatures.

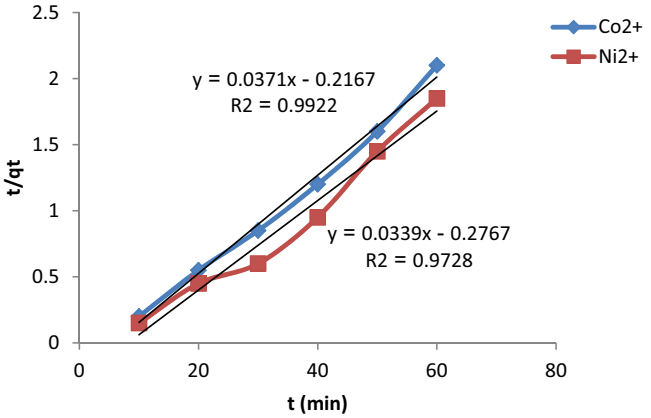

Fig. 13. Pseudo-second-order model for the sorption of Ni(II) and Co(II) ions onto *Origanum majorana*-capped AgNPs. [Ni(II) and Co(II) ions concentration = 30 mg/L, pH = 9.0 Ni(II) ion and pH = 7.0 Co(II) ion, adsorbent dose = 0.05 g, stirring speed = 180 rpm, and temperature = 25°C].

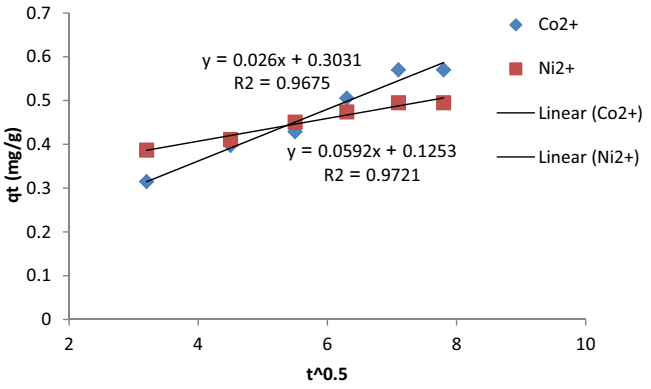

Fig. 14. Elovich model for the sorption of Ni(II) and Co(II) ions onto *Origanum majorana*-capped AgNPs. [Ni(II) and Co(II) ions concentration = 30 mg/L, pH = 9.0 Ni(II) ion and pH = 7.0 Co(II) ion, adsorbent dose = 0.05 g, stirring speed = 180 rpm, and temperature = 25°C].

The estimation of $\Delta G°$ values was done applying the equation adsorption of Ni(II) and Co(II) ions. As shown in Fig. 15, the exothermicity nature of the process was apparent since, with an increase in the temperature from 298 to 348 K, *O. majorana*-capped AgNPs adsorbent abated. With the help of the plots, the calculation of the values of the thermodynamic parameters (Tables 5 and 6) [40] was carried out. The negative value of $\Delta G°$ well-expressed the viability and spontaneity nature of the process. On the other hand, the negative value of $\Delta H°$ revealed the exothermicity nature of adsorption. Also, the value of $\Delta S°$ was a fine sign of alter in the randomness at the derived *O. majorana*-capped AgNPs solution interface during the sorption. It has been reported as a fact that $\Delta G°$ values up to –2.858 kJ/mol Ni(II) ions and –1.035 kJ/mol Co(II) ions confirm with electrostatic interaction between sorption sites and the Ni(II) and Co(II) ions (physical adsorption). In the sorption process, the predominance of the physical sorption mechanism was confirmed from the obtained $\Delta G°$ values for Ni(II) and Co(II) ions (<–5 kJ/mol).

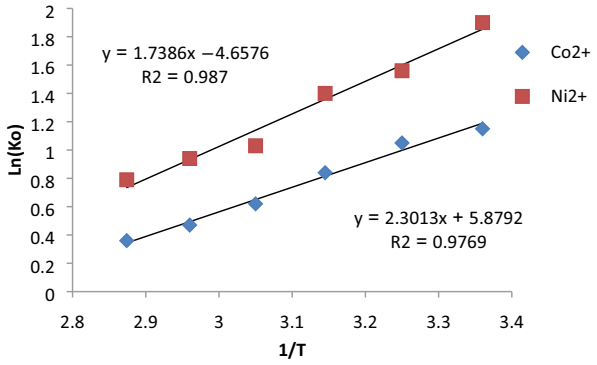

Fig. 15. Plot of $\ln K_c$ vs. $1/T$ for the assessment of thermodynamic parameters. [Ni(II) and Co(II) ions concentration = 30 mg/L, pH = 9.0 Ni(II) ion and pH = 7.0 Co(II) ion, adsorbent dose = 0.05 g, contact time = 60 min, and stirring speed = 180 rpm].

3.10. Adsorption mechanism of Ni(II) and Co(II) ions into O. majorana-capped AgNPs

The physical and chemical characteristics of *O. majorana*-capped AgNPs were substantially changed by calcination. The specific surface area and the amount of polar functional groups increased, and the adsorption performance improved [40]. Overall, the mechanisms of adsorption of Ni(II) and Co(II) ions onto *O. majorana*-capped AgNPs were mainly attributed to two aspects: chemical adsorption and physical adsorption. Under acid conditions, chemical adsorption is dominant. The carboxyl of Ni(II) and Co(II) ions undergoes ion and/or proton exchange reactions with the reactive sites of AgNPs-AC with hydroxyl groups. Hydroxyl groups on the adsorbent combine with H^+ in solution, thus resulting in a greater hydroxyl group exchange and the formation of ($-OH_2^+$), according to Eqs. (A). Furthermore, proton exchange reactions occur between $-OH_2^+$ and the hydroxyl group with outer complexes (Eqs. (B) and (C)). Finally, the inner complex is formed by ligand exchange, according to Eqs. (D) and (E).

$$\text{Ag NP}_S\text{-AC} - \text{OH} + \text{H}^+ \rightarrow \text{Ag NP}_S\text{-AC} - \text{OH}_2^+ \quad \text{(A)}$$

$$\text{Ag NP}_S\text{-AC} - \text{OH}_2^+ + \text{Ni}^{2+} - \text{C(O)O}^- \leftrightarrow \text{AR} - \text{OH}_2^+\text{O}^- - \text{C(O)} - \text{Ni}^{2+} \quad \text{(B)}$$

$$\text{Ag NP}_S\text{-AC} - \text{OH}_2^+ + \text{Co}^{2+} - \text{C(O)O}^- \leftrightarrow \text{AR} - \text{OH}_2^+\text{O}^- - \text{C(O)} - \text{Co}^{2+} \quad \text{(C)}$$

$$\text{Ag NP}_S\text{-AC} - \text{OH}_2^+\text{O}^- - \text{C(O)} - \text{Ni}^{2+} \leftrightarrow \text{Ag NP}_S\text{-AC} - \text{OC(O)} - \text{Ni}^{2+} + \text{H}_2\text{O} \quad \text{(D)}$$

$$\text{Ag NP}_S\text{-AC} - \text{OH}_2^+\text{O}^- - \text{C(O)} - \text{Co}^{2+} \leftrightarrow \text{Ag NP}_S\text{-AC} - \text{OC(O)} - \text{Co}^{2+} + \text{H}_2\text{O} \quad \text{(E)}$$

In neutral and weak alkaline conditions, Ni(II) and Co(II) ions exhibit a substantial proton loss and exist as free ions in solution, thus inhibiting the chemical adsorption to some extent. However, the porous structure of AgNPs-AC

Table 5
Distribution coefficients at diverse temperature. [Ni(II) and Co(II) ions concentration = 30 mg/L, pH = 9.0 Ni(II) ion and pH = 7.0 Co(II) ion, adsorbent dose = 0.05 g, contact time = 60 min, and stirring speed = 180 rpm]

Ions concentration (mg/L)	R^2	K_D					
		298 K	308 K	318 K	328 K	338 K	348 K
Ni(II) ions 30 (mg/L)	0.987	3.17	2.76	2.33	1.87	1.62	1.43
Co(II) ions 30 (mg/L)	0.9769	8.09	4.88	3.55	3.27	2.57	2.13

Table 6
Thermodynamic parameters for the adsorption of Ni(II) and Co(II) ions onto *Origanum majorana*-capped AgNPs sorbent. [Ni(II) and Co(II) ions concentration = 30 mg/L, pH = 9.0 Ni(II) ion and pH = 7.0 Co(II) ion, adsorbent dose = 0.05 g, contact time = 60 min, and stirring speed = 180 rpm]

Ions concentration (mg/L)	$\Delta H°$ (kJ/mol)	$\Delta S°$ (kJ/mol K)	$\Delta G°$ (kJ/mol)					
			298 K	308 K	318 K	328 K	338 K	348 K
Ni(II) ions 30 (mg/L)	–14.455	–38.683	–2.858	–2.6	–2.236	–1.706	–1.356	–1.035
Co(II) ions 30 (mg/L)	–21.65	–56.4	–5.18	–4.06	–3.35	–3.24	–2.653	–2.188

especially after modification tempers the negative effect via physical adsorption.

3.11. Recycling of the adsorbent

The ability to recovering and reusing of the adsorbent was tested in several steps of adsorption and desorption [41]. The result is shown in Fig. 16. As shown in Fig. 16, 88/6 of nickel and cobalt ions were desorbed from the adsorbent after first cycle and after four cycles, there were slight changes in nickel and cobalt ions desorption. So, it was concluded that the desired removal of 90% can be achieved after four cycles.

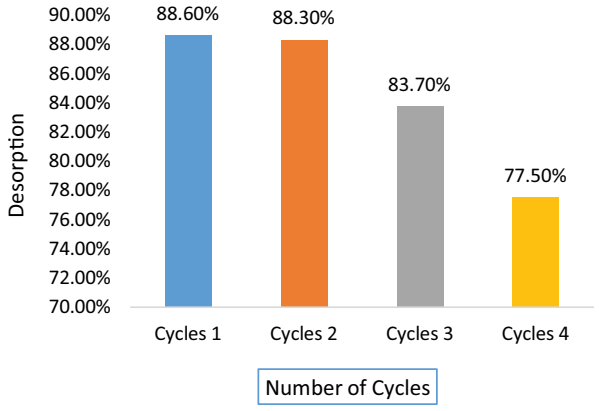

Fig. 16. Desorption of Ni(II) and Co(II) from the adsorbent after tree cycles. [Ni(II) and Co(II) ions concentration = 30 mg/L, pH = 9.0 Ni(II) ion and pH = 7.0 Co(II) ion, adsorbent dose = 0.05 g, contact time = 60 min, and stirring speed = 180 rpm].

3.12. Juxtaposition of O. majorana-capped AgNPs adsorption method outcomes with those of other methods

Table 7; demonstrates the max adsorption capacities of varied adsorbents for the deletion of Ni(II) and Co(II) ions comparatively. The type and density of active sites in adsorbents which are responsible for adsorption of metal ions from the solution result in the variation in (q_{max}) values. The outcomes of the table clearly show that the sorption capacity of utilized *O. majorana*-capped AgNPs in the current study is significantly high. In general, morphology, particle size and distribution, and surface structure of this sorbent were effective in its successful outcomes.

4. Conclusion

The selection of *O. majorana* functionalized with silver nanoparticles as an efficacious adsorbent for the deletion of Ni(II) and Co(II) ions from aqueous solutions has been scrutinized. In this current article, the applicability of *O. majorana*-capped AgNPs as an available, useful, and affordable material for deleting Ni(II) and Co(II) ions from aqueous media has been confirmed. The desired values of the pH, adsorbent dosage, Ni(II), and Co(II) ions concentration, and contact time were found to be pH of 9.0 for Ni(II) and pH of 7.0 for Co(II) ions, 40 and 50 mg for Ni(II) and Co(II) ions, 30 mg/L, and 60 min for adsorption of Ni(II) and Co(II) ions into *O. majorana* functionalized with silver nanoparticles. Studying the impact of various process parameters revealed that when initial Ni(II) and Co(II) ions concentration increased, percent adsorption decreased but percent adsorption enhanced when adsorbent dosage enhanced. The highest Ni(II) and Co(II) ions deletion by the adsorbent occurred at pH of 9.0 for Ni(II) and pH of 7.0 for Co(II) ions. The maximum adsorption capacities (q_{max}) were found to be 180.0 and 130.5 mg/g for Ni(II) and Co(II) ions into *O. majorana* functionalized with silver nanoparticles, respectively. Equilibrium adsorption showed that system followed Langmuir model. The kinetics scrutiny decided that Ni(II) and Co(II) ions deletion comply with the pseudo-second-order rate equation. At the temperatures under

Table 7
Juxtaposition of the adsorption capacities of different adsorbents for removal Ni(II) and Co(II)

Metal ions	Adsorbent	Adsorption capacity (mg/g)		References
		Ni(II)	Co(II)	
Co(II)	Corn cob micro powder	–	6.62	[5]
Ni(II), Co(II), Zn(II)	Modified *Aspergillus flavus* biomass	32.26	31.06	[8]
Cu(II), Co(II)	Modified marine algae	–	13.73	[9]
Pb(II), Co(II)	CaO/Fe_3O_4 magnetic composite	–	217.39	[26]
Ni(II)	Graphene/δ-MnO_2 composite	52.1	–	[32]
Ni(II)	Fe_3O_4 nano particles modified by oak shell	454.5	–	[41]
Co(II), Cd(II)	Geraphene oxide (GO)	–	68.20	[42]
Ni(II), Co(II)	Carboxylated nanoporous graphene	94.34	87.72	[43]
Co(II), Mn(II)	Maize cob activated carbon	–	9.35	[44]
Ni(II), Cd(II), Pb(II), Cr(III)	Activated carbon prepared from *Cucumis melo* peel	23.80	–	[45]
Ni(II), Co(II)	Oxalate modified activated carbon	52.63	50.76	[46]
Ni(II), Co(II)	*Origanum majorana*-capped AgNPs	180.0	130.5	Present study

investigation, spontaneous adsorption of Ni(II) and Co(II) ions was reported. Also, the exothermicity of the sorption process was confirmed by the negative values of ($\Delta G°$, $\Delta H°$, and $\Delta S°$). Besides the likelihood of recycling the adsorbent was well-proved by desorption studies. Based on the results from the linear regression-based analysis, it was revealed that the derived empirical models represented a passable prediction of performance into *O. majorana* functionalized with silver nanoparticles with significant determination coefficients (R^2 = 0.9922–0.9728). Additionally, the statistical outcomes guaranteed that the recommended equations could favorably be employed for the adsorption of Ni(II) and Co(II) ions from aqueous solutions. Further investigations on the suitability of this adsorbent for the deletion of other materials have been suggested. Also, it was suggested to make inquiries about the suitability of this adsorbent in industrial applications. The findings proved the appropriateness of the present procedure for the successful deletion of pollutants from aqueous solution.

Acknowledgments

The authors would like to acknowledge that the research was partially supported by the Islamic Azad University, Branch of Omidiyeh Iran.

References

[1] S. Sobhanardakani, R. Zandipak, 2,4-Dinitro phenyl hydrazine functionalized sodium dodecyl sulfate-coated magnetite nanoparticles for effective removal of Cd(II) and Ni(II) ions from water samples, J. Environ. Monit. Assess., 187 (2015) 412–419, doi: 10.1007/s10661-015-4635-y.
[2] S. Sobhanardakani, K. Jamshidi, Assessment of metals (Co, Ni and Zn) content in the sediments of mighan wetland using geo-accumulation index, Iran. J. Toxicol., 9 (2015) 1386–1390.
[3] M. Nasr, A. El Din Mahmoud, M. Fawzy, A. Radwan, Artificial intelligence modeling of cadmium(II) biosorption using rice straw, Appl. Water Sci., 7 (2017) 823–831.
[4] M. Yasmin Regina, S. Saraswathy, B. Kamal, V. Karthik, K. Muthukumaran, Removal of nickel(II) ions from wastewater using low cost adsorbents: a review, J. Chem. Pharm. Sci., 8 (2015) 1–6.
[5] G.H. Haghdoost, The use of corn cob micro powder as a low cost adsorbent, for the removal of Co^{2+} ion from aqueous solutions and from the view point thermodynamics, J. Phys. Theor. Chem., 15 (2018) 105–212.
[6] Y. Saghapour, M. Aghaie, K. Zare, H. Aghai, Cobalt(II) ion removal by adsorption onto graphene nanosheets: kinetic and thermodynamic studies, Ind. J. Fundam. Appl. Life Sci., 4 (2014) 1469–1478.
[7] S. Sobhanardakani, Ecological and human health risk assessment of heavy metal content of atmospheric dry deposition, a case study, Biol. Trace Elem. Res., 187 (2019) 602–610.
[8] R. Foroutan, H. Esmaeili, S.D. Rishehri, F. Sadeghzadeh, S. Mirahmadi, M. osarifard, B. Ramavandi, Zinc, nickel, and cobalt ions removal from aqueous solution and plating plant wastewater by modified *Aspergillus flavus* biomass: a dataset, Data Brief, 12 (2017) 485–492.
[9] R. Foroutan, H. Esmaeili, M. Abbasi, M. Rezakazemi, M. Mesbah, Adsorption behavior of Cu(II) and Co(II) using chemically modified marine algae, J. Environ. Technol., 39 (2018) 2792–2800.
[10] B. Kakavandi, A. Raofi, S.M. Peyghambarzadeh, B. Ramavandi, M. Hazrati Niri, M. Ahmadi, Efficient adsorption of cobalt(II) Ion on chemical modified activated carbon: characterization, optimization and modeling studies, Desal. Water Treat., 111 (2018) 310–321.
[11] F. Manal, N. Mahmoud, A. Samar, N. Heba, H. Shacker, Environmental approach and artificial intelligence for Ni(II) and Cd(II) biosorption from aqueous solution using *Typha domingensis* biomass, Ecol. Eng., 95 (2016) 743–752.
[12] W. Konicki, I. Pełech, E. Mijowska, Removal of Ni^{2+} from aqueous solutions by adsorption onto magnetic multi walled carbon nanotube nanocomposite, Pol. J. Chem. Technol., 16 (2014) 87–94.
[13] S. Sobhanardakani, R. Zandipak, Synthesis and application of $TiO_2/SiO_2/Fe_3O_4$ nanoparticles as novel adsorbent for removal of Cd(II), Hg(II) and Ni(II) ions from water samples, Clean. Technol. Environ. Policy, 19 (2017) 1913–1925.
[14] A.A. Basaleh, M.H. Al-Malack, T.A. Saleh, Metal removal using chemically modified eggshells: preparation, characterization, and statistical analysis, Desal. Water Treat., 173 (2020) 313–330.
[15] S. Pandey, G.K. Goswami, K.K. Nanda, Green synthesis of biopolymer–silver nanoparticle nanocomposite: an optical sensor for ammonia detection, Int. J. Biol. Macromol., 51 (2012) 583–589.

[16] A. Syafiuddin, Salmiati, M.R. Salim, A.B.H. Kueh, T. Hadibarata, H. Nur, A review of silver nanoparticles: research trends, global consumption, synthesis, properties, and future Challenges, J. Clin. Chem. Soc., 64 (2017) 732–756.
[17] L. Zhou, H. Kamyab, A. Surender, A. Maseleno, N. Kaeachi, Z. Parsaee, Novel Z-scheme composite Ag_2CrO_4/NG/polymide as high performance nano catalyst for photoreduction of CO_2: design, fabrication, characterization and mechanism, J. Photochem. Photobiol., 368 (2019) 30–40.
[18] S. Pandey, G.K. Goswami, K.K. Nanda, Green synthesis of biopolymer-silver nanoparticle nanocomposite: an optical sensor for ammonia detection, Int. J. Biol. Macromol., 51 (2012) 583–589.
[19] V.K. Gupta, O. Moradi, I. Tyagi, S. Agarwal, H. Sadegh, R.S. Ghoshekandi, A.S.H. Makhlouf, M. Goodarzi, A. Garshasbi. Study on the removal of heavy metal ions from industry waste by carbon nanotubes: effect of the surface modification: a review, Crit. Rev. Environ. Sci. Technol., 46 (2016) 93–118.
[20] A.C. Burdușel, O. Gherasim, A.M. Grumezescu, L. Mogoanta, A. Ficai, E. Andronescu, Biomedical applications of silver nanoparticles, Nanomaterials, 8 (2018) 681–693, doi: 10.3390/nano8090681.
[21] J.S. Justin Packia Jacob, A.N. Finub, Synthesis of silver nanoparticles using *Piper longum* leaf extracts and its cytotoxic activity against Hep-2 cell line, Colloids Surf., B, 91 (2012) 212–214.
[22] P.K. Singh, K. Bhardwaj, P. Dubey, A. Prabhune, UV-assisted size sampling and antibacterial screening of *Lantana camara* leaf extract synthesized silver nanoparticles, RSC Adv., 5 (2015) 24513–24520.
[23] A. Dehghanpoor Frashah, S. Hashemian, F. Tamadon, Ag doped hydroxyapatite nano particles for removal of methyl red azo dye from aqueous solutions kinetic and thermodynamic studies, Eur. J. Anal. Chem., 15 (2020) 32–44.
[24] Y.H. Chen, C.S. Yeh, A new approach for the formation of alloy nanoparticles: laser synthesis of gold–silver alloy from gold–silver colloidal mixtures electronic supplementary information (ESI) available: experimental details, UV-VIS spectra, TEM images and EDX analysis for molar ratios (Au:Ag) of 1:2 and 2:1, Chem. Commun., 2001 (2001) 371–372.
[25] C. Krishnaraj, E.G. Jagan, S. Jagan, P. Rajasekar, P.T. Selvakumar, N. Kalaichelvan, Synthesis of silver nanoparticles using *Acalypha indica* leaf extracts and its antibacterial activity against water borne pathogens, Colloids Surf., B, 76 (2010) 50–56.
[26] F. Shakerian Khoo, H. Esmaili, Synthesis of CaO/Fe_3O_4 magnetic composite for the removal of Pb(II) and Co(II) from synthetic wastewater, J. Serb. Chem. Soc., 83 (2018) 237–249.
[27] C. Cheng, W. Wang, X. Yang, A. Li, C. Philippe, Adsorption of Ni(II) and Cd(II) from water by novel chelating sponge and the effect of alkali-earth metal ions on the adsorption, J. Hazard. Mater., 264 (2014) 332–341.
[28] X. Guo, B. Du, Q. Wei, J. Yang, L. Hu, L. Yan, W. Xu, Synthesis of amino functionalized magnetic graphenes composite material and its application to remove Cr(VI), Pb(II), Hg(II), Cd(II) and Ni(II) from contaminated water, J. Hazard. Mater., 278 (2014) 211–220.
[29] L.F. Muhaisen, Nickel ions removal from aqueous solution using sawdust as adsorbent: equilibrium, kinetic and thermodynamic studies, J. Eng. Sustainable Dev., 21 (2017) 60–72.
[30] M. Fawzy, M. Nasr, S. Helmi, H. Nagy, Experimental and theoretical approaches for Cd(II) biosorption from aqueous solution using *Oryza sativa* biomass, Int. J. Phytorem., 18 (2016) 1096–1103.
[31] I. Langmuir, The constitution and fundamental properties of solids and liquids. Part I. Solids, J. Am. Chem. Soc., 38 (1916) 2221–2295.
[32] Y. Ren, N. Yan, Q. Wen, Z. Fan, T. Wei, M. Zhang, J. Ma, Graphene/δ-MnO_2 composite as adsorbent for the removal of nickel ions from wastewater, J. Chem. Eng., 175 (2011) 1–7.
[33] D. Bulgariu, L. Bulgariu, Equilibrium and kinetics studies of heavy metal ions biosorption on green algae waste biomass, Bioresour. Technol., 103 (2012) 489–493.
[34] T.K. Kim, T. Kim, W.S. Choe, M.K. Kim, Y.J. Jung, Removal of heavy metals in electroplating wastewater by powdered activated carbon (PAC) and sodium diethyldithiocarbamate-modified PAC, J. Environ. Eng. Res., 23 (2018) 301–308.
[35] M.A. Khan, M. Ngabura, T.S. Choong, Biosorption and desorption of nickel on oil cake: batch and column studies, Bioresour. Technol., 103 (2012) 35–42.
[36] E.C. Salihi, J. Wang, D.J.L. Coleman, L. Siller, Enhanced removal of nickel(II) ions from aqueous solutions by SDS-functionalized graphene oxide, J. Sep. Sci. Technol., 51 (2016) 1317–1327.
[37] P.S. Kumar, K. Kirthika, Equilibrium and kinetic study of adsorption of nickel from aqueous solution onto bael tree leaf powder, J. Eng. Sci. Technol., 4 (2009) 351–363.
[38] V. Jonasi, K. Matina, U. Guyo, Removal of Pb(II) and Cd(II) from aqueous solution using alkaline-modified pumice stone powder (PSP): equilibrium, kinetic, and thermodynamic studies, Turk. J. Chem., 41 (2017) 748–759.
[39] R. Prabakaran, S. Arivoli, Adsorption kinetics, equilibrium and thermodynamic studies of nickel adsorption onto *Thespesia populnea* bark as biosorbent from aqueous solutions, Eur. J. Appl. Eng. Sci. Res., 1 (2012) 134–142.
[40] S. Mustapha, D.T. Shuaib, M.M. Ndamitso, M.B. Etsuyankpa, A. Sumaila, U.M. Mohammed M.B. Nasirudeen, Adsorption isotherm, kinetic and thermodynamic studies for the removal of Pb(II), Cd(II), Zn(II) and Cu(II) ions from aqueous solutions using *Albizia lebbeckpods*, Appl. Water Sci., 9 (2019) 142–153.
[41] S.M. Mousavi, S.A. Hashemi, H. Esmaeili, A.M. Amani, F. Mojoudi, Synthesis of Fe_3O_4 nano particles modified by oak shell for treatment of wastewater containing Ni(II), Acta Chim. Slov., 65 (2018) 750–756.
[42] G. Zhao, J. Li, X. Ren, C. Chen, X. Wang, Few-layered graphene oxide nanosheets as superior sorbents for heavy metal ion pollution management, Environ. Sci. Technol., 45 (2011) 10454–10462.
[43] A. Khaligh, H. Zavvar Mousavi, A. Rashidi, Ultrasonic assisted removal of Ni(II) and Co(II) ions from aqueous solutions by carboxylated nanoporous graphene, J. Appl. Chem., 11 (2017) 49–58.
[44] G.B. Adebayo, H.I. Adegoke, W. Jamiu, B.B. Balogun, A.A. Jimoh, J. Appl. Sci. Environ. Manage., 19 (2015) 737–748.
[45] M. Manjuladevi, R. Anitha, S. Manonmani, Kinetic study on adsorption of Cr(VI), Ni(II), Cd(II) and Pb(II) ions from aqueous solutions using activated carbon prepared from *Cucumis melo* peel, Appl. Water Sci., 8 (2018) 36–44.
[46] H. Kasaini, P.T. Kekana, A.A. Saghti, K. Bolton, Proceedings of World Academy of Science, Engineering and Technology, World Acad. Sci. Eng. Technol., 159 (2013) 707–716.